Extreme Mechanics Letters 45 (2021) 101297

Contents lists available at ScienceDirect

Extreme Mechanics Letters

journal homepage: www.elsevier.com/locate/eml

Machine-learning optimized method for regional control of sound fields

Tianyu Zhao, Yiwen Li, Lei Zuo *, Kai Zhang *

School of Aerospace Engineering, Beijing Institute of Technology, Beijing, 100081, China

ARTICLE INFO

Article history:
Received 2 January 2021
Received in revised form 6 March 2021
Accepted 23 March 2021
Available online 29 March 2021

Keywords:
Machine learning
Regional control
Local sound field
Metasurface

ABSTRACT

Acoustic wave control is an important issue in living environment. Designing metasurface on scatterers is expected to control the sound field. However, an effective method to design the metasurface for large regional control is still lacking. Here we propose a machine-learning optimized method to solve problem of designing metasurface. According to the relationship between sound pressures at multiple points, convolutional neural network (CNN) is used to establish the mapping from local sound field to phase gradient of metasurface, which is further optimized by another CNN. The machine-learning method on designing metasurface has higher accuracy than the genetic algorithm. Using the machine-learning optimized method, not only the phase gradient of the metasurface can be obtained according to sound field, but also regional control of local sound field can be realized. For example, we can realize 8.37 dB intensification and 1.50 dB weakening of sound field at a square with a half-wavelength side. The metasurface designed by our proposed method is expected to realize noise reduction in large space, opening an avenue to achieve complex wave manipulation.

1. Introduction

Acoustic wave control is an important issue in living environment [1]. The propagation of acoustic wave can be controlled by using acoustic metasurfaces with sub-wavelength thickness [2,3]. The metasurface has become an effective method for modulating phase of scatterings, leading to various applications, such as focusing reflected waves [4], acoustic diffusers [5], holography [6], acoustic communication [7,8], and shaping reverberating fields [9]. To realize various functionalities, we need design the phase gradients of metasurfaces. Analytical methods are widely used to design the phase gradient of metasurfaces in case the target sound field can be described analytically, such as planer acoustic lens [4] and negative refraction [10]. In addition, feedback iterative algorithm from optics [11–13] has been used for designing the phase gradients of metasurfaces, which control sound field at a single point in reverberating field [9] or along limited lines for acoustic holography [14]. However, regional control of local sound field, which consists of sound pressures/phases at multiple points, has not been reported in the literature.

In fact, the control of local sound field at multiple points is hindered by conventional methods (analytical method and feedback iterative algorithm). For the analytical method, it is difficult to establish an analytical model in local sound fields to solve phase gradients of metasurfaces. For feedback iterative algorithm [9–12], there exists large time consumption. However, the sound pressures/phases at multiple points are dependent, whose internal relationship is ignored by conventional methods. Machine learning (ML) is a mathematical tool to find relationships in big data [15,16] and has been widely used in physics [17–19], data science [20], computer vision [21], medical imaging-based diagnosis [22], and strategic games [23]. In the field of electromagnetic wave, machine learning can optimize three-dimensional chiral metamaterials [24] and design metasurfaces [25–27]. In the field of sound wave, machine learning can speed up the optimization of bandgap design of acoustic tetrachiral metamaterials [28]. However, machine learning has not been used to design the phase gradients of acoustic metasurfaces. Here we propose a machine-learning optimized method to obtain phase gradient of the metasurface according to the functionalities of controlling sound field. Using this proposed method, regional control of local sound field including intensification/weakening can be realized, which has the advantage of accuracy and no problem of divergence (see Fig. 1).

2. Methods

The proposed machine-learning optimized method contains three steps: data generation, training machine learning model to predict metasurface, optimizing the phase gradient of the metasurface according to desired functionality.

* Corresponding authors.
E-mail addresses: zuolei@bit.edu.cn (L. Zuo), zhangkai@bit.edu.cn (K. Zhang).

https://doi.org/10.1016/j.eml.2021.101297

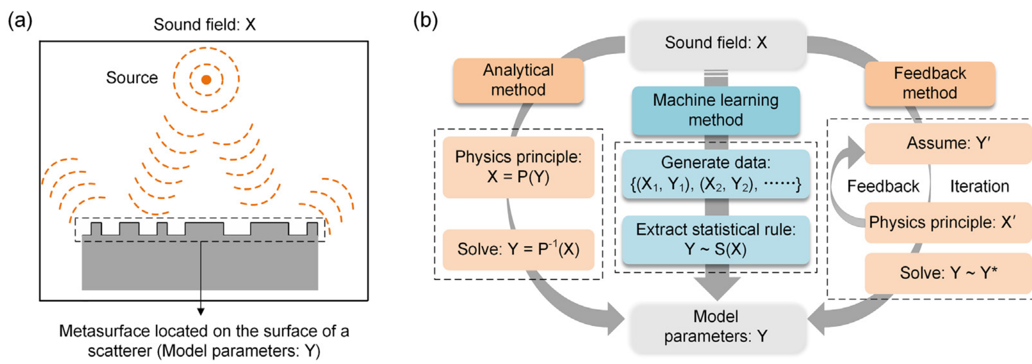

Fig. 1. Acoustic wave control with a reflective metasurface and the procedure for designing phase gradient of metasurface. (a) A sound source excites the sound field (X) in space and the sound wave is reflected from the metasurface (model parameter: Y). (b) Three solutions to designing the phase gradient of metasurface: analytic method, feedback method and machine learning method.

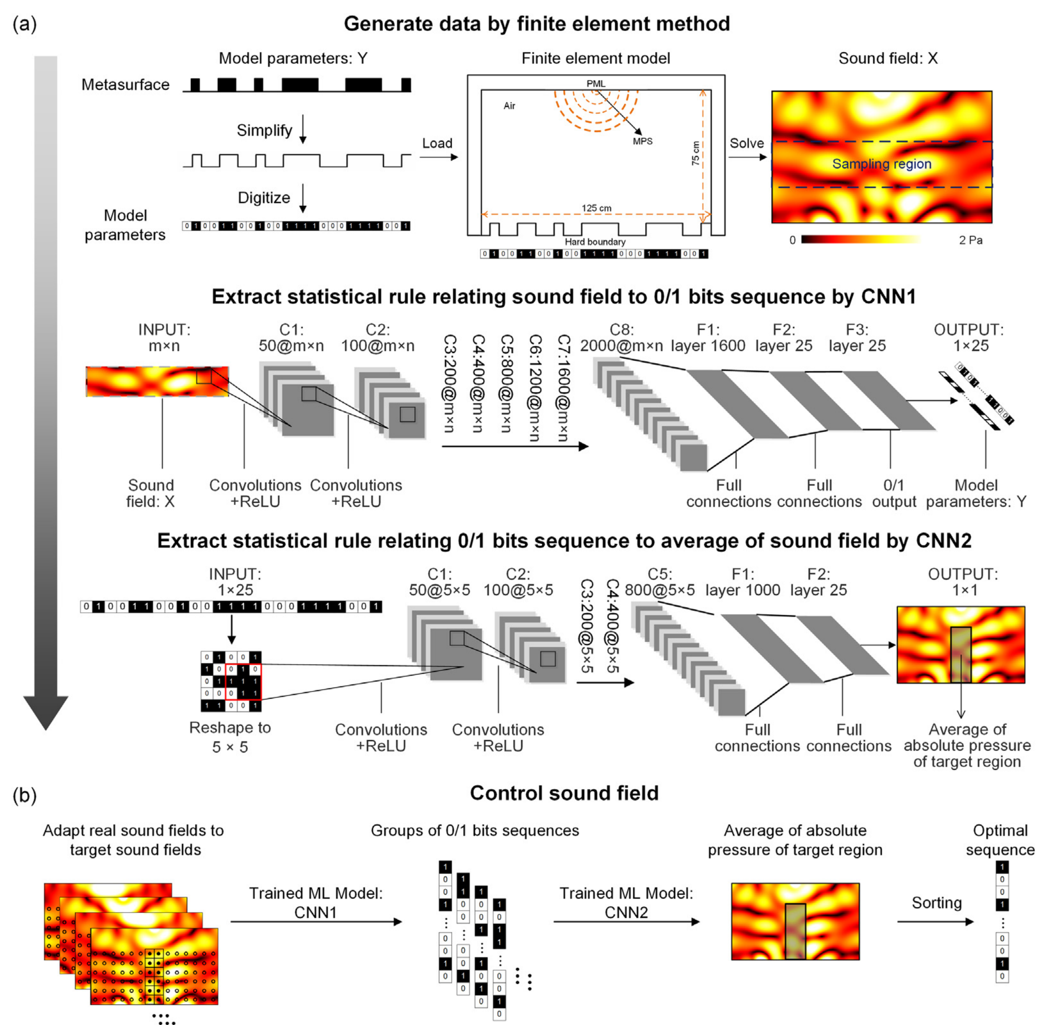

Fig. 2. Applying machine learning to control sound field. (a) A phase gradient consisting of 0/1-bits is randomly generated. Finite element method is used to calculate sound fields with different binary sequences of the metasurface. CNN1 is established to predict the sequence of metasurface according to sound field. CNN2 is established to predict the average value of sound pressure field in target region according to sequence. (b) Procedure of machine-learning optimized method.

Step 1: Finite element method is used to generate a mass of reliable data on absolute sound pressure fields and phase gradients of the metasurfaces, as shown in Fig. 2a. We first digitize the phase gradient of a metasurface into a 0/1-bit sequence based on the concept of digital metamaterials [25,29–31]. We build an acoustic metasurface with the dimensions of 125 cm × 4 cm, whose unit is a rectangle channel with the dimensions of 5 cm × 4 cm. The acoustic wave can enter the channel and be reflected from the bottom called “0” bit or be reflected from the top called “1” bit, so that the metasurface can be described as a binary sequence. We then establish a 75 cm × 125 cm 2D airborne sound field in the simulation software COMSOL 5.2. Three perfectly matched layers (PMLs) are applied on the upper, left, and right boundaries, respectively. The lower boundary is

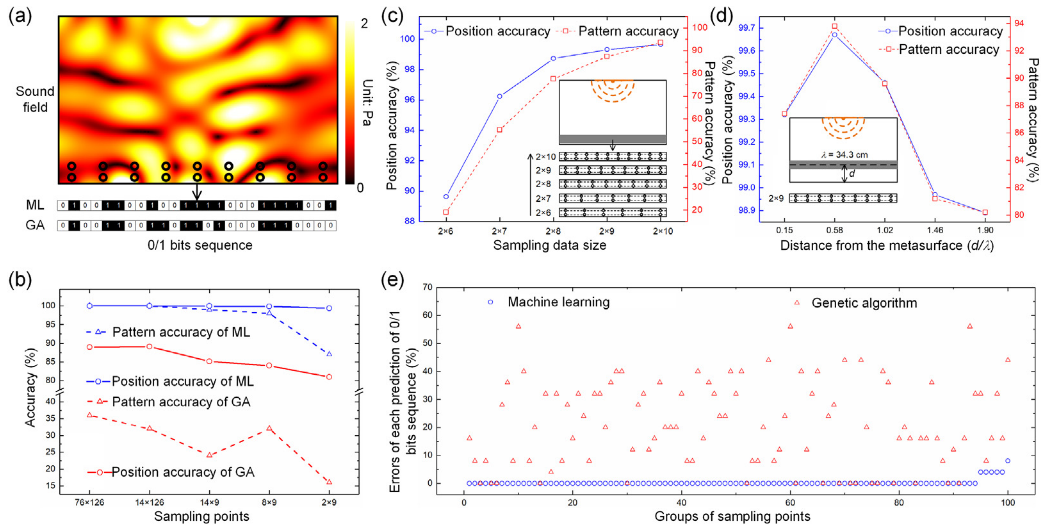

Fig. 3. Comparisons between machine learning and genetic algorithm on 0/1-bit sequence prediction. (a) Input, 2 × 9 points of sound field. The ML and GA are then used to predict 0/1-bit sequences. (b) Changes in accuracy with size of sampled data in the same sampling region. (c) Changes in accuracy with distance between sampling region and the metasurface. (d) Changing the size of input sound fields and using ML and GA to predict the 0/1-bit sequence of 100 and 25 groups of sound fields to obtain average accuracies, respectively. (e) Inputting 100 groups of 2 × 9 points of sound fields, using the ML and GA to predict the 0/1-bit sequences, and counting errors between the predicted and real sequences.

the metasurface. A monopole point sound source (MPS) with a frequency of 1000 Hz, amplitude of 1 Pa, and phase zero rad is applied at the center of the upper boundary. In the acoustic modeling, the acoustic velocity and density of air are assumed to be 343 m/s and 1.29 kg/m^3. We use MATLAB R2017b to randomly generate 250,000 groups of binary sequences of length 25 as the 0/1 patterns of metasurfaces, then solve and save corresponding absolute sound pressure fields for convolutional neural networks (CNNs) training.

Step 2: CNN1 model is proposed to establish the relationships from sound field to metasurface, which is built with Google's TensorFlow deep learning framework [32]. We use PyCharm Community edition (2018.3) to run all Python codes of the CNN models. The CNN1 model contains one input layer, four or eight convolutional layers, two full connected layers and one output layer. The input is the absolute sound pressure field and the output is the 0/1-bit sequence of metasurface. The number of feature maps of each convolutional layer is set as 50, 100, 200, 400, 800, 1200, 1600, and 2000 in order. The convolutional kernel size is chosen as 3 × 3. For each convolutional layer, we choose Rectified Linear Unit (ReLU) as the activation function. As shown in Fig. 2a, after the convolutional layers and two full connected layers (F1 and F2), a piecewise constant function ($f(x) = 0$, when $x < 0.5$; $f(x) = 1$, when $x \geq 0.5$) is used in the output layer (F3) to map the output of F2 to a binary sequence, which is the pattern of metasurface predicted by CNN1 according to targeted sound pressure field. The training set contains 200,000 groups of data, and the test set contains 50,000 groups of data. Taking the local field in Fig. 2a as an example, after 103 epochs, the rate of position accuracy, defined as the ratio of the number of all precisely predicted bits to the total number of bits in the test set, is 99.32%. Among the results, we further count all precisely predicted 0/1-bit sequences and divide the number by the total number of 0/1-bit sequences in the test set. This ratio defined as the rate of pattern accuracy is 87.4%. More details are in **Supplementary Material**.

Step 3: To find the optimal binary sequence for sound field control, we establish a second convolutional neural network called CNN2. To consider the 0/1-bit sequence as 2D data, we reshape it from 1 × 25 to 5 × 5. CNN2 model is proposed here to establish the relationship from metasurface to sound field. The CNN2 model consists of one input layer, five convolutional layers, two fully connected layers and one output layer. The input is the 0/1-bit sequence of metasurface and the output is average absolute sound pressure of target region. Here, we use the average absolute sound pressure as characteristic of the target region. The number of feature maps of each convolutional layer is 50, 100, 200, 400 and 800 in order. The convolutional kernel size is chosen as 3 × 3. ReLU is used as the activation function. We define loss and maximum error to evaluate the training effectiveness of CNN2. The loss is the average difference between predicted value and real value. Maximum error is the maximum difference between predicted value and real value in the test set. Taking the binary sequence in Fig. 2a as an example, after 624 epochs, the loss is 1.6×10^{-3} Pa and the maximum error is 0.01 Pa.

After training CNN1 and CNN2, we can obtain optimal target sound field by changing 0/1-bit sequence, as shown in Fig. 2b. Groups of numerical real sound fields, which are from the database of sound fields calculated by FEM, are adapted to unreal sound fields, via multiplying the absolute pressure of sound field in the target region by a constant. Groups of the adapted sound fields are input into CNN1 to obtain groups of 0/1-bit sequences, which are then input into CNN2 to predict the average values of sound pressure fields of the target region. By sorting the average values, the optimal 0/1-bit sequence of metasurface is finally found according to the functionality of intensification/weakening. More details are in **Supplementary Material**.

3. Results

We study the influence of the coverage, density, and position of sampling points on accuracies. The results are shown in Fig. 3. We sample the entire sound field, and 76 × 126 points (height × width) form the densest sampling points, where the space between these points along the height and width is 1 cm, much smaller than the wavelength ($\lambda = 34.3$ cm). Both rates of position and pattern accuracy for 76 × 126 points are 100%. We increase the space of sampling points and obtain 100% accuracies for 14 × 126 sampling points and even remaining 99% pattern accuracy for 14 × 9. Afterwards, we sample local sound field by keeping the sampling space unchanged and reducing the height. For 8 × 9 sampling points, the pattern accuracy reduces to 98%. For minimum height of 2 × 9, the pattern accuracy is 87%. Namely, even if we only sample two points in the height direction, we can still get high accuracy by sampling enough points along the width. Furthermore, we study the influence of the density of sampling points on accuracies, as shown in Fig. 3b. The number of sampling points varies from 2 × 10 to 2 × 6. As the density of sampling point decreases, the position accuracy reduces from 99.66% to 89.63%, while pattern accuracy reduces from 93.6% to 19.0%. The larger region of sound field covered by the sampling points and the denser sampling points, the higher accuracy we can get. Lastly, the impact of position of the sampling region on the accuracies is also investigated. As shown in Fig. 3c, for a total of 2 × 9 points, we change the distance (d) between the sampling region and the metasurface from 0.15λ (5 cm) to 1.9λ (65 cm). As the distance increases, both accuracies decrease, especially pattern accuracy, which decreases to 80.2% at the distance equal to 1.9λ. Thus, using local sound fields close to the metasurface can satisfy the requirement of high accuracies.

Secondly, we compare the accuracy and efficiency of ML method with that of genetic algorithm (GA). Genetic algorithm is an optimization algorithm that searches for the global optimal solution or approaches it and does not need the derivative of the objective function [33]. GA is used to predict 25 groups of 0/1-bit sequences with different numbers of sampling points. As shown in Fig. 3d, the accuracies of GA decrease sharply with decreasing number of sampling points. For GA, the position accuracy for 76 × 126 points of sound fields, is (88.96 ± 12.13) % and pattern accuracy is 36%, decreasing to (80.96 ± 15.20) % and 16% for 2 × 9 points of sound fields, respectively. To further compare the capability of ML and GA to predict the 0/1-bit sequence, we choose 2 × 9 sampling points of the 10 cm × 125 cm sound fields, where ML exhibits relative "low" accuracy compared with sampling denser points. We predict 100 groups of 0/1-bit sequences using the two methods, and the errors are shown in Fig. 3e. The accuracy of ML method is high and stable, whereas that of GA is very low and unstable. For each prediction, ML takes average time of 7×10^{-4} seconds and GA takes average time of 2.4×10^{4} seconds. The ML method exhibits consistently fast, which means that the well-trained ML method is suitable for real-time control of sound field at a large scale.

Finally, based on the advantages of machine-learning optimized method, acoustic metasurface is designed to control regional sound field. We investigate the ability of weakening/intensification of sound field near/far from the metasurface, respectively. The area of the target region increases from 1 × 1 to 4 × 4 boxes (9 cm × 9 cm for each box). When the target region is near from the metasurface, as shown in Fig. 4a, the absolute pressure with 1 × 1 box can be intensified by 8.37 dB or weakened by 1.50 dB on average, compared with the reference sound field (Fig. 4c). As the target regions increase in size to 4 × 4 boxes, the effect of intensification decreases to 1.06 dB, while that of weakening increases to 2.30 dB. When the target region is far from the metasurface (Fig. 4b), as the corresponding area increases, the weakening effect decreases from 3.69 dB to 1.97 dB, and the intensification effect decreases from 1.74 dB to 0.21 dB. For target regions with the same area, the range of control effect near the metasurface is always larger than that far from the metasurface.

We provide specific controlled sound fields to intuitively show the regional control effect. We can achieve a 32.84 dB reduction of the sound pressure at a given point (Fig. S5). For regional control, the sound field of target region in Fig. 4d,e is intensified by 2.59 dB and 1.69 dB, respectively, and that in Fig. 4f is weakened by 2.31 dB. Other controlled sound fields are shown in Fig. S6. We can control local sound field in a large region, which has not been realized before.

In practice, sound-absorbing materials can be used to absorb sound energy and reduce noise. Based on our proposed machine-learning optimized method, the energy distribution of the sound field can be manipulated by adjusting the phase gradient of multi-functional metasurface, then sound-absorbing materials are placed in the region of energy concentration to maximize the efficiency of sound absorption. Noise reduction in some public places, such as trains, offices, airplanes, and theaters, where there is a corridor for walking and people stay on the two sides of the corridor, is one typical scenario. As shown in Fig. S7, we use two pieces of sound-absorbing materials in the middle where energy concentrated, then weaken the sound field on two sides. Sound-absorbing materials can only influence energy distribution of local field near them, while the energy distribution of entire sound field can be tailored by using designed metasurface. By combining sound-absorbing materials with metasurface technology, both the maximum and average pressure of the entire target region are weakened. For example, the maximum absolute sound pressure is further weakened by 1.72 dB in the entire target region, compared with only using sound-absorbing materials. Prominently, a local region with 1× 3 boxes (9 cm × 27 cm), which is highlighted in red line, can be weakened by 4.12 dB. We can also adjust the positions of two pieces of sound-absorbing materials slightly, then weaken sound field on one side, as shown in Fig. S8. In this way, a quieter but smaller region can be created. The maximum absolute sound pressure in the weakened region is 0.75 Pa, weakened up to 2.7 dB.

Although our proposed metasurface is based on the data of sound fields with the source of 1000 Hz, this metasurface is still applicable to control sound fields of other frequencies. Namely, when the sound source is broadband, the 0/1 sequence obtained by CNNs can still control regions of sound field. We show the broadband effect of the machine-learning metasurface for regional control in Fig. 5 and Figs. S8-11. As shown in Fig. 5, the sound energy in the central 6 × 2 boxes is concentrated with source frequency ranging from 500 to 2000 Hz, compared with the reference fields at corresponding frequencies. It means that the machine-learning optimized method is extraordinary suitable for controlling sound fields of multiple frequencies, which are common in scenarios such as offices and venues. However, it can be drawn that the intensification/weakening effect diminishes as the frequency moves far away from 1000 Hz, where active approaches are needed for better broadband effect, such as piezoelectric actuators [34].

4. Conclusions

In summary, we propose a machine-learning optimized method to design the phase gradient of acoustic metasurface for regional control of local sound field. In this method, CNNs are used to exploit the relationship between sound pressures at multiple points to solve the problem of inversely designing metasurface. Using the machine-learning optimized method, not only the binary sequence of the metasurface can be obtained according to local sound field, but also regional control of sound field including intensification and weakening can be realized. The machine learning method exhibits excellent accuracy in obtaining the phase gradients of metasurfaces according to local sound field, which is significantly better than genetic algorithm. The metasurface designed by the machine-learning optimized method has potential applications for noise reduction, which opens an

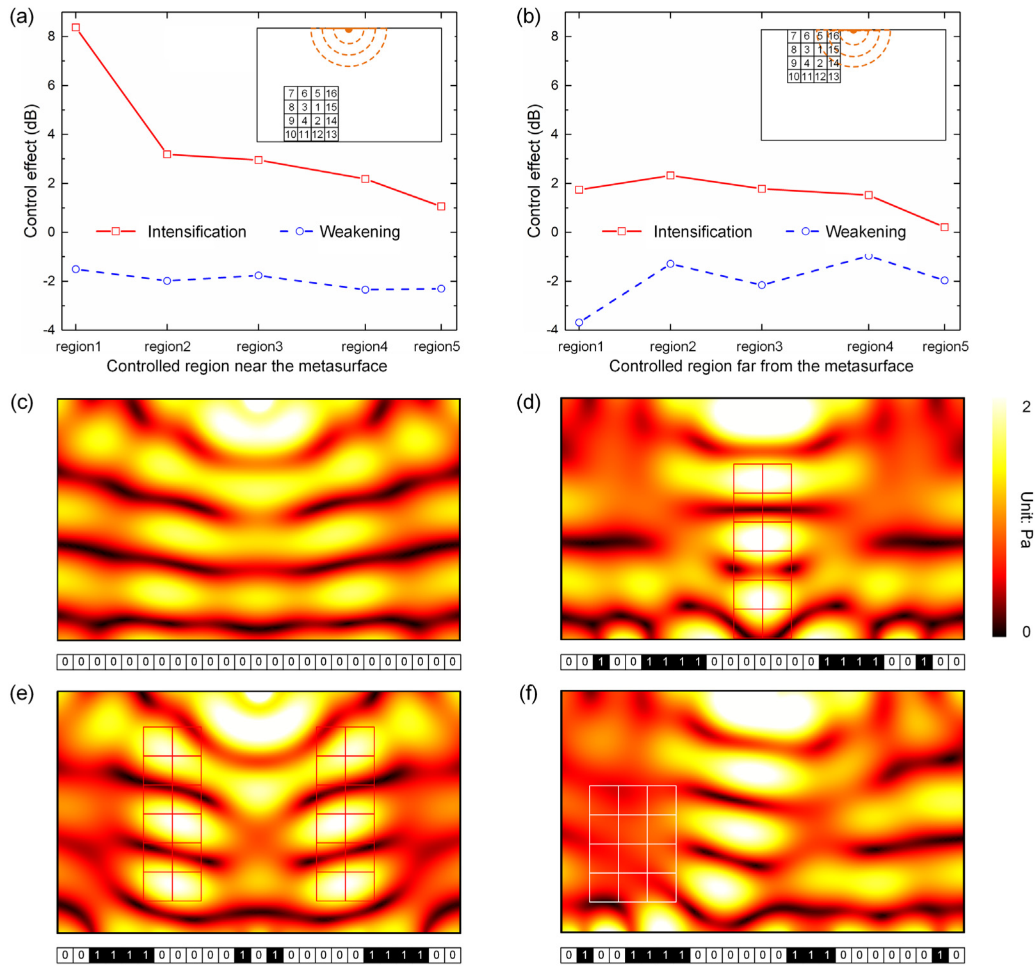

Fig. 4. Regional control of sound field and the corresponding 0/1-bit sequence. (a) The control effect changes with the increase in the area of target region near the metasurface. (b) The control effect changes with the increase in the area of target region far from the metasurface. (Region 1 contains box 1, region 5 contains all boxes, regions 2, 3, 4 contain boxes 1∼2, 1∼4, and 1∼9, respectively.) (c) Reference sound field with a sequence of all zero-bits. (d) Sound energy is concentrated in the middle. (e) Sound energy is concentrated on both sides. (f) Sound energy is reduced in the lower-left region.

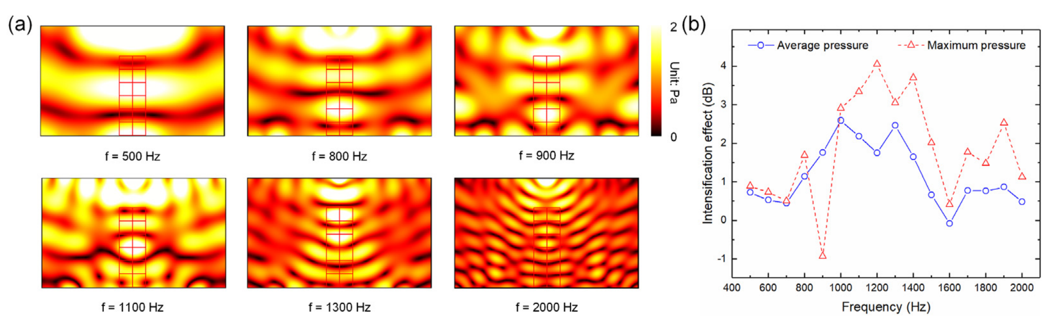

Fig. 5. Broadband effect of intensification in the middle. (a) Sound fields are intensified in the central 6 × 2 boxes. (b) Intensification effect with the source frequency ranging from 500 to 2000 Hz.

avenue to design more complex manipulation of sound field on demand.

CRediT authorship contribution statement

Tianyu Zhao: Developed the method, Built the numerical program, Carried out the numerical computation, Writing the paper. **Yiwen Li:** Developed the method, Built the numerical program, Writing the paper. **Lei Zuo:** Developed the method, Writing the paper. **Kai Zhang:** Proposed the key idea, Developed the method, Writing the paper.

Declaration of competing interest

The authors declare that they have no known competing financial interests or personal relationships that could have appeared to influence the work reported in this paper.

Data availability

The authors declare that all other relevant data supporting the findings of this study are available within the Article and its Supplementary Material files, or from the corresponding author on reasonable request.

Acknowledgments

This work has been supported by the National Natural Science Foundation of China (Grants No. 11991030 and No. 11991031) and the China Postdoctoral Science Foundation (grant No. 2020M680014).

Appendix A. Supplementary data

Supplementary material related to this article can be found online at https://doi.org/10.1016/j.eml.2021.101297. See supplementary material for details of CNN1 and CNN2, genetic algorithm, controlling sound field at a point, weakening the sound fields, reducing noise by combining metasurfaces and sound-absorbing materials and broadband effect of regional control.

References

[1] P. Sheng, Introduction to Wave Scattering, Localization and Mesoscopic Phenomena, Academic Press, San Diego, 1995.
[2] S.A. Cummer, J. Christensen, A. Alù, Controlling sound with acoustic metamaterials, Nat. Rev. Mater. 1 (2016) 16001, http://dx.doi.org/10.1038/natrevmats.2016.1.
[3] B. Assouar, B. Liang, Y. Wu, Y. Li, J.-C. Cheng, Y. Jing, Acoustic metasurfaces, Nat. Rev. Mater. 3 (2018) 460–472, http://dx.doi.org/10.1038/s41578-018-0061-4.
[4] Y. Li, X. Jiang, R. Li, B. Liang, X. Zou, L. Yin, J. Cheng, Experimental realization of full control of reflected waves with subwavelength acoustic metasurfaces, Phys. Rev. Appl. 2 (2014) 064002, http://dx.doi.org/10.1103/PhysRevApplied.2.064002.
[5] Y. Zhu, X. Fan, B. Liang, J. Cheng, Y. Jing, Ultrathin acoustic metasurface-based schroeder diffuser, Phys. Rev. X 7 (2017) 021034, http://dx.doi.org/10.1103/PhysRevX.7.021034.
[6] Y. Xie, C. Shen, W. Wang, J. Li, D. Suo, B.-I. Popa, Y. Jing, S.A. Cummer, Acoustic holographic rendering with two-dimensional metamaterial-based passive phased array, Sci. Rep. 6 (2016) 35437, http://dx.doi.org/10.1038/srep35437.
[7] X. Jiang, B. Liang, J. Cheng, C. Qiu, Twisted acoustics: metasurface-enabled multiplexing and demultiplexing, Adv. Mater. 30 (2018) 1800257, http://dx.doi.org/10.1002/adma.201800257.
[8] C. Shi, M. Dubois, Y. Wang, X. Zhang, High-speed acoustic communication by multiplexing orbital angular momentum, Proc. Natl. Acad. Sci. USA 114 (2017) 7250–7253, http://dx.doi.org/10.1073/pnas.1704450114.
[9] G. Ma, X. Fan, P. Sheng, M. Fink, Shaping reverberating sound fields with an actively tunable metasurface, Proc. Natl. Acad. Sci. USA 115 (2018) 6638–6643, http://dx.doi.org/10.1073/pnas.1801175115.
[10] Y. Xie, W. Wang, H. Chen, A. Konneker, B.-I. Popa, S.A. Cummer, Wavefront modulation and subwavelength diffractive acoustics with an acoustic metasurface, Nat. Commun. 5 (2014) 5553, http://dx.doi.org/10.1038/ncomms6553.
[11] S. Mellin, G. Nordin, Limits of scalar diffraction theory and an iterative angular spectrum algorithm for finite aperture diffractive optical element design, Opt. Express 8 (2001) 705–722, http://dx.doi.org/10.1364/OE.8.000705.
[12] I.M. Vellekoop, Feedback-based wavefront shaping, Opt. Express 23 (2015) 12189–12206, http://dx.doi.org/10.1364/OE.23.012189.
[13] R. Di Leonardo, F. Ianni, G. Ruocco, Computer generation of optimal holograms for optical trap arrays, Opt. Express 15 (2007) 1913–1922, http://dx.doi.org/10.1364/OE.15.001913.
[14] K. Melde, A.G. Mark, T. Qiu, P. Fischer, Holograms for acoustics, Nature 537 (2016) 518–522, http://dx.doi.org/10.1038/nature19755.
[15] M.I. Jordan, T.M. Mitchell, Machine learning: Trends, perspectives, and prospects, Science 349 (2015) 255–260, http://dx.doi.org/10.1126/science.aaa8415.
[16] Y. LeCun, Y. Bengio, G. Hinton, Deep learning, Nature 521 (2015) 436–444, http://dx.doi.org/10.1038/nature14539.
[17] M. Raissi, P. Perdikaris, G.E. Karniadakis, Physics-informed neural networks: A deep learning framework for solving forward and inverse problems involving nonlinear partial differential equations, J. Comput. Phys. 378 (2019) 686–707, http://dx.doi.org/10.1016/j.jcp.2018.10.045.
[18] M.A. Bessa, S. Pellegrino, Design of ultra-thin shell structures in the stochastic post-buckling range using Bayesian machine learning and optimization, Int. J. Solids Struct. 139–140 (2018) 174–188, http://dx.doi.org/10.1016/j.ijsolstr.2018.01.035.
[19] S. Tang, L. Zhang, W.K. Liu, From virtual clustering analysis to self-consistent clustering analysis: a mathematical study, Comput. Mech. 62 (2018) 1443–1460, http://dx.doi.org/10.1007/s00466-018-1573-x.
[20] P. Raccuglia, K.C. Elbert, P.D.F. Adler, C. Falk, M.B. Wenny, A. Mollo, M. Zeller, S.A. Friedler, J. Schrier, A.J. Norquist, Machine-learning-assisted materials discovery using failed experiments, Nature 533 (2016) 73–76, http://dx.doi.org/10.1038/nature17439.
[21] O. Russakovsky, J. Deng, H. Su, J. Krause, S. Satheesh, S. Ma, Z. Huang, A. Karpathy, A. Khosla, M. Bernstein, A.C. Berg, L. Fei-Fei, ImageNet large scale visual recognition challenge, Int. J. Comput. Vis. 115 (2015) 211–252, http://dx.doi.org/10.1007/s11263-015-0816-y.
[22] A. Esteva, B. Kuprel, R.A. Novoa, J. Ko, S.M. Swetter, H.M. Blau, S. Thrun, Dermatologist-level classification of skin cancer with deep neural networks, Nature 542 (2017) 115–118, http://dx.doi.org/10.1038/nature21056.
[23] D. Silver, J. Schrittwieser, K. Simonyan, I. Antonoglou, A. Huang, A. Guez, T. Hubert, L. Baker, M. Lai, A. Bolton, Y. Chen, T. Lillicrap, F. Hui, L. Sifre, G. van den Driessche, T. Graepel, D. Hassabis, Mastering the game of Go without human knowledge, Nature 550 (2017) 354–359, http://dx.doi.org/10.1038/nature24270.
[24] W. Ma, F. Cheng, Y. Liu, Deep-learning-enabled on-demand design of chiral metamaterials, ACS Nano 12 (2018) 6326–6334, http://dx.doi.org/10.1021/acsnano.8b03569.
[25] L. Li, H. Ruan, C. Liu, Y. Li, Y. Shuang, A. Alù, C.-W. Qiu, T.J. Cui, Machine-learning reprogrammable metasurface imager, Nat. Commun. 10 (2019) 1082, http://dx.doi.org/10.1038/s41467-019-09103-2.
[26] Z. Liu, D. Zhu, S.P. Rodrigues, K.-T. Lee, W. Cai, Generative model for the inverse design of metasurfaces, Nano Lett. 18 (2018) 6570–6576, http://dx.doi.org/10.1021/acs.nanolett.8b03171.
[27] C.C. Nadell, B. Huang, J.M. Malof, W.J. Padilla, Deep learning for accelerated all-dielectric metasurface design, Opt. Express 27 (2019) 27523–27535, http://dx.doi.org/10.1364/OE.27.027523.
[28] A. Bacigalupo, G. Gnecco, M. Lepidi, L. Gambarotta, Machine-learning techniques for the optimal design of acoustic metamaterials, J. Optim. Theory Appl. (2019) http://dx.doi.org/10.1007/s10957-019-01614-8.
[29] C. Della Giovampaola, N. Engheta, Digital metamaterials, Nat. Mater. 13 (2014) 1115–1121, http://dx.doi.org/10.1038/nmat4082.
[30] Z. Wang, Q. Zhang, K. Zhang, G. Hu, Tunable digital metamaterial for broadband vibration isolation at low frequency, Adv. Mater. 28 (2016) 9857–9861, http://dx.doi.org/10.1002/adma.201604009.
[31] T.J. Cui, M.Q. Qi, X. Wan, J. Zhao, Q. Cheng, Coding. metamaterials, Coding metamaterials digital metamaterials and programmable metamaterials, Light-Sci. Appl. 3 (2014) e218, http://dx.doi.org/10.1038/lsa.2014.99.
[32] M. Abadi, P. Barham, J. Chen, Z. Chen, A. Davis, J. Dean, M. Devin, S. Ghemawat, G. Irving, M. Isard, M. Kudlur, J. Levenberg, R. Monga, S. Moore, D.G. Murray, B. Steiner, P. Tucker, V. Vasudevan, P. Warden, M. Wicke, Y. Yu, X. Zheng, TensorFlow: A system for large-scale machine learning, in: Proc. 12th USENIX Conference on Operating Systems Design and Implementation, Savannah, GA, USA, Berkeley, CA, USA, 2016, pp. 265–283, http://dl.acm.org/citation.cfm?id=3026877.3026899 (accessed September 2, 2019).
[33] D.E. Goldberg, J.H. Holland, Genetic algorithms and machine learning, Mach. Learn. 3 (1988) 95–99, http://dx.doi.org/10.1023/A:1022602019183.
[34] X. Li, Y. Chen, R. Zhu, G. Huang, An active meta-layer for optimal flexural wave absorption and cloaking, Mech. Syst. Signal Process. 149 (2021) 107324, http://dx.doi.org/10.1016/j.ymssp.2020.107324.